

Modelling of cavitation in water saturated porous media considering effects of dissolved air

Dariusz Gawin¹

Department of Building Physics and Building Materials, Technical University of Lodz
Al. Politechniki 6, 90-924 Lodz, Poland, e-mail: gawindar@p.lodz.pl

Lorenzo Sanavia

Dipartimento di Costruzioni e Trasporti, Università degli Studi di Padova
Via Marzolo 9, 35-131 Padova, Italy, e-mail: lorenzo.sanavia@unipd.it

Dedicated to Professor Bernhard A. Schrefler on the occasion of his 65th birthday

Abstract. An extension of a mathematical model for non-isothermal multiphase materials to consider the dissolution of air in liquid water and air mass sources during its desorption at lower water pressure is presented. The solid skeleton is assumed elasto-plastic; heat, water and air flows and water phase changes are taken into account. Physics of air dissolution and water cavitation in porous media is discussed. A numerical example where cavitation develops during strain localization in undrained water saturated dense sands is solved with the developed model as discretized in space and time with the Finite Element Method.

Keywords: Poromechanics, Multiphase porous material, Coupled Thermo-Hydro-Mechanical model, Air dissolution and desorption, Water cavitation, Strain localization.

1 Introduction

In recent years, increasing interest in thermo-hydro-mechanical analysis of saturated and partially saturated materials is observed, because of a wide spectrum of their engineering applications. Typical examples belong to environmental geomechanics, where some challenging problems are of interest, and among them, those due to soil failure situations caused by shear bands development.

Strain localization in water saturated geomaterials has been modelled in recent years e.g. by Rudnicki and Rice (1975), Vardoulakis (1986), Shuttle and Smith (1990), Chambon *et al.* (1994), Schrefler *et al.* (1995), Schrefler *et al.* (1996), Gawin *et al.* (1998), Ehlers and Volk

(1999), Zhang *et al.* (2001), Borja (2004), Ehlers *et al.* (2004), Mira *et al.* (2004), Sanavia *et al.* (2006) among others.

There are also experimental results available, e.g. in the works of Mokni and Desrues (1998), Vardoulakis and Sulem (1995) and McManus and Davis (1997). The case of undrained tests on dense (i.e. dilatant) sand samples are interesting because the experimental results show that the water pressure decreases continuously almost from the beginning on. At the onset of localization this pressure is decisively smaller than the atmospheric pressure and is close to the cavitation pressure. This pressure was always reached at the onset of localization, irrespectively of the back pressure at the beginning of the experiment, and cavitation was observed. Cavitation, i.e. liquid water phase change to vapour, initiates in fully water saturated porous media when the absolute pressure of liquid water is equal to or smaller than the saturation vapour pressure at the temperature of surrounding water (neglecting the surface tension on the interface of the arising gas bubbles). Then desaturation of the porous material may take place if capillary pressure develops. The process can be accelerated by release of the air dissolved in liquid water.

Usually the above mentioned experiments are performed by saturating the specimens with de-aired water and making circulate fresh de-aired water in order to dissolve the rest of gas bubbles possibly trapped in the specimens and the circuits (Mokni and Desrues, 1998). In field conditions this is however not the case. The question how the air dissolved in water can influence the evolution of cavitation during strain localization is an important motivation for development of the proposed model. In fact, the low value of water pressure observed during strain localization in water saturated dense sands, causes a release of certain amount of air dissolved in water because the solubility of air in liquid water, according to Henry's law, equation (1), decreases proportionally to the pressure drop (Figure 2). For example 1 dm³ of sand, saturated with water and having porosity of 20%, may contain at 20°C maximally about 3.98 ml of dissolved (dry) air at atmospheric pressure ($p_{atm}= 101325$ Pa) and only 0.09 ml of water vapour at pressure of 2339 Pa (i.e. saturated vapour pressure at 20 °C). The excess amount of air is released in the form of small air bubbles. The process starts when the actual volume concentration of air dissolved in liquid water is equal to the equilibrium one corresponding to the actual water pressure. Hence release of air dissolved in liquid water may be indicated as a triggering mechanism for cavitation, as was shown by Baur *et al.* (1998) for the case of cavitation inception in free surface flows.

¹ Corresponding author

Cavitation in water saturated dense sand samples with impervious boundary was analyzed numerically by Schrefler *et al.* (1996) and Gawin *et al.* (1998), where the so-defined *isothermal monospecies approach* and the *isothermal two phase flow model* have been developed by neglecting the heat effects of phase change of liquid water to vapour. These effects were taken into account in the non-isothermal three-phase model developed by Sanavia *et al.* (2006), where it was assumed that water vapour was the only gas present in pores at cavitation.

In this paper we extend the previous mathematical model of Sanavia *et al.* (2006) by considering, as a novel aspect, the air dissolved in pore water and its release to the gas phase after a liquid water pressure drop. Our aim is to analyse numerically the effect of air released during the desaturation initiated by cavitation due to strain localisation.

Most mathematical and finite element models of coupled hydro-thermo-mechanical (CHTM) phenomena in porous media, also those used in Geomechanics for analyses of soil behaviour at various conditions, (e.g. Gawin and Schrefler, 1996; Ehlers and Volk, 1999; Lewis and Schrefler, 1998; Schrefler 2002; Borja 2004; Ehlers *et al.*, 2004), do not consider the air dissolved in pore water. A general CHTM model considering air dissolved in the pore water has been theoretically formulated by Olivella *et al.* (1994) and Khalili and Loret (2001). A numerical solution has been presented in the work of Gens *et al.* (1998), where the behaviour of deep nuclear waste disposal was analyzed, concluding that the contribution of air dissolved in CTHM modelling is negligible for that kind of problems. To the authors' knowledge, no previous attempt was made to study the influence of dissolved air on the progress of cavitation at strain localization.

The paper is organized as follows. Physics of air dissolution in fully and partially water saturated porous media and its contribution to water cavitation are discussed in Section 2 and 3, respectively. By recalling the classical nucleation theory for gaseous bubble formation, it will be explained how the presence of bubbles of dissolved air is an important factor that could trigger cavitation in porous media. Moreover, the amount of air which can be released to cavitation bubbles will be estimated.

Then, in Section 4 the mathematical model for a non-isothermal multiphase porous media including dissolution of air in water is derived at macroscopic level. The multiphase medium is considered as an elasto-plastic porous continuum where heat, water and gas flow are taken into account. The gas phase is modelled as an ideal gas composed of dry air (including air released from water) and water vapour, considered as two miscible species. Small strains and

quasi-static loading conditions are assumed. For the numerical solution, the developed model has been simplified by neglecting advection and diffusion of released air.

Finally, a finite element simulation is presented in Section 5 to analyze numerically the effect of the released air on the initiation and progress of cavitation during strain localization in undrained water saturated dense sands. It will be shown that the release of dissolved air is of importance during simulation of cavitation and subsequent desaturation process.

A possible engineering application of the model is the analysis of onset of a rapid landslide when vaporization of pore water could be generated by frictional heating in the failure zone (as in case of Vajont landslide, Hendron and Patton, 1985 following the work of Habib, 1975) Another possible application is the simulation of the THM behaviour of earth dams, as suggested by LeBihan and Leroueil (2002) to describe the unexpected pore pressures observed in the core of some earth dams.

2 Dissolution of air in fully and partially saturated porous media

It is commonly believed that atmospheric air dissolves in ground water at the water table. But the significant excess of atmospheric noble gases observed in the liquid water, as compared to the solubility equilibrium concentrations, (Mercury *et al.*, 2004), shows that there are also other air dissolution mechanisms. Those are, in general, related to the dissolution of the air bubbles trapped in pores of water saturated soils during seasonal fluctuations of water table, and to the direct dissolution of air in a partially water saturated ground (Mercury *et al.*, 2004). Gas dissolution in water at equilibrium conditions can be described by Henry's law in the following form, (Atkins and de Paula 2002),

$$p_i^g = K_{xi} \cdot x_i = K_{ci} \cdot c_i, \quad (1)$$

where p_i^g means the partial pressure of the gas component i , x_i and c_i are the mol fraction and concentration of the gas i in liquid water at equilibrium, K_{xi} and $K_{ci} = K_{xi} \cdot M_w / (\rho^w \cdot M_i)$ are the empirical Henry's law constants, related to the mol fraction of gas component i in liquid water, $x_i = n_i / n_w$, or its concentration, $c_i = m_i / V_w$, respectively. M_w and M_i are molar masses, while n_w and n_i quantities of liquid water and dissolved gas, expressed in moles, ρ^w the water density and V_w the water volume. $x_i = n_i / n_w = m_i M_w / (M_a m_w)$.

As can be observed in Figure 1, the value of Henry's law constant depends both on the water pressure and temperature, p^w and T , (Mercury *et al.*, 2004). Figure 1 clearly shows, that as pressure and/or temperature of water are increasing, the Henry's law constant increases as

well, (Mercury *et al.* 2003), hence the concentration of gas i dissolved in liquid water, at equilibrium with gas of a given pressure, p_i^g , decreases.

A total change of concentration of the gas i dissolved in water, dc_i , can be calculated from the following relation,

$$dc_i = \frac{dp_i^g}{K_{ci}} - \frac{p_i^g}{(K_{ci})^2} \left(\frac{\partial K_{ci}}{\partial p^w} dp^w + \frac{\partial K_{ci}}{\partial T} dT \right). \quad (2)$$

Thus, at constant gas pressure ($dp_i^g=0$) and temperature ($dT=0$), the concentration c_i at equilibrium with gas of pressure p_i^g decreases if water pressure is lowered because $\frac{\partial K_{ci}}{\partial p^w}$ is positive, Figure 1.

When a dissolving gas consists of several components, like for example atmospheric air does, one can apply Henry's law to each of them separately and then sum up the contributions of all components considering their partial pressures. Using the thermodynamic data given by Mercury *et al.* (2003) and assuming that dry air consists in 21% of Oxygen and 79% of Nitrogen, the 'apparent' values of Henry's law constants for the dry air have been calculated for different temperatures and pressures of liquid water, see Figure 1.

When pressure of water, containing initially the equilibrium concentration of dissolved air, decreases, an excess amount of the air is liberated in the form of air bubbles, as will be explained in next section. The gas pressure in these bubbles is equal to the sum of the water pressure, p^w , and the pressure exerted by a curved gas–water interface due to surface tension, $p^c=2\sigma_{wa}/R_b$, where σ_{wa} means the liquid water-air interfacial tension and R_b is the radius of the curvature. The latter pressure, for bubbles with radius greater than 10^{-4} m, has a value smaller than $p^c=1.445$ kPa, which is negligible as compared to the atmospheric pressure, and hence also to the water pressure. Thus, assuming for simplicity, that the gas pressure inside the air bubbles is equal to the water pressure, $p^a \cong p^w$, and the Henry's law coefficient is independent of pressure, $K_{wa} = const$, one can assess a rate at which the concentration of air dissolved in water is changing as follows,

$$\frac{\partial c_{wa}}{\partial t} = \frac{1}{K_{wa}} \frac{\partial p^w}{\partial t}. \quad (3)$$

This clearly shows that effects related to the dissolved air may be particularly of importance when a fast water pressure decrease occurs.

In principle, Henry's law is applicable to water at positive pressures and in several textbooks of Physics or Chemistry one can find the values of Henry's law constant for different gases at various pressure and temperature, see e.g. Atkins and de Paula (2002). However, it is commonly known that capillary water is exposed to negative pressures, i.e. it is stretched, and hence it exists in a metastable state, (Mercury and Tardy, 2001, 2004; Zheng *et al.*, 1991), which is thermodynamically possible up to the so called spinodal limit, i.e. the extreme tensile strength of water, for example -212.4 MPa at temperature of 30°C (Mercury *et al.*, 2004). Applicability of Henry's law, and especially values of its constant (measured at $p^w > 0$), also for capillary water is disputable, because experimental studies are possible only for positive water pressures (Mercury and Tardy 2004). During cavitation in porous media we deal with water pressures which are relatively close to zero, and Figure 1 shows that in this range of pressure the value of Henry's law constant is practically dependent on temperature only. With this assumption, using Henry's law (1) and data shown in Figure 1, the gas pressure dependence of solubility of air in liquid water ($p^w = 1\text{kPa}$) at different three different temperatures has been plotted in Figure 2.

Figure 1 and Figure 2

3 Physics of cavitation in fully saturated soils

An influence of dissolved air on the initiation of cavitation and further desaturation in water saturated soils will be briefly summarized here from the microscopic point of view. This will be not directly used in our model, but gives a deeper insight in physics of the phenomena dealt with in the paper.

From the Classical Nucleation Theory, it is concluded that cavitation at low stretching pressures cannot be practically initiated by thermal fluctuations (Maris and Balibar, 2000). In such conditions, the most important factor which could trigger cavitation nucleation in soils is the presence of impurities or air bubbles in water (Or and Tuller, 2002; Maris and Balibar, 2000; Tyree 1997), because only bubbles with radius greater than the critical value, R_c , can grow freely (i.e. without energy supply) and can seed cavitation. The critical radius of air bubbles in water is given by the following equation (see Figure 3),

$$R_c = \frac{2\sigma_{wa}}{p^g - p^w}. \quad (4)$$

For any critical radius and water pressure, taking into account the solubility of air in liquid water, one can assess the desaturation degree caused by the air mass released from liquid water after a decrease of water pressure to the value necessary to form gas bubbles of critical sizes and to start cavitation (Figure 4). For example, in this figure it can be seen that, after a decrease of water pressure to the value $p^w = -1$ kPa, for bubbles with radius $R_c = 4 \cdot 10^{-3}$ m one obtains an additional water desaturation $\Delta S_w = 4.55\%$. For larger bubbles the value of desaturation ΔS_w is greater, e.g. for $R_c = 6 \cdot 10^{-3}$ m, one obtains $\Delta S_w = 8.56\%$

Figure 3 and Figure 4

Thus it may be concluded that desorption of air from water saturated with dissolved air, after the onset of cavitation in soils, can cause faster water desaturation, affecting the evolution of the process. These phenomena will be simulated in Section 5 by means of the proposed numerical CHTM model.

It should be underlined that the presented theory and analyses have a simplified character, because they assume an immediate air dissolution – desorption, and in reality the rate of these processes is finite, and furthermore there are some associated diffusion flows of dissolved air, which influence their time evolution (Kwak and Kim 1998). Then, the presented theory does not take into account influence of the porous structure upon the onset of cavitation.

4 Macroscopic balance equations

The full mathematical model necessary to simulate thermo-hydro-mechanical transient behaviour of fully and partially saturated porous media, neglecting air dissolved in water, was developed by Gawin and Schrefler (1996), Lewis and Schrefler (1998) and Schrefler (2002) using averaging theories according to Hassanizadeh and Gray (1979). Elasto-plasticity was introduced in the work of Sanavia *et al.* (2006). The underlying physical model is described in Schrefler (2002) and will be summarized here for sake of completeness.

The partially saturated porous medium is treated as multiphase system composed of the solid skeleton (s) and voids filled with water (w) and gas (g). The latter is assumed to behave as an ideal mixture of two species: dry air (noncondensable gas, ga) and water vapour (condensable one, gw).

At the macroscopic level the porous media material is modelled by a substitute continuum that simultaneously fills the entire domain, where each constituent π has a reduced density

which is obtained through the volume fraction $\eta^\pi(\mathbf{x},t) = dv^\pi(\mathbf{x},t) / dv(\mathbf{x},t)$, where \mathbf{x} is the vector of the spatial coordinates and t is the current time. In the model, heat conduction and convection, vapour diffusion, water flow due to pressure gradients or capillary effects and water phase change (evaporation and condensation) inside the pores are taken into account. The solid is deformable and non-polar, and the fluids, solid and thermal fields are coupled. All fluids are in contact with the solid phase. The constituents are assumed to be isotropic, homogeneous, immiscible except for dry air and water vapour, and chemically non-reacting. Solid and liquid water constituents are incompressible at micro level, while gas is considered compressible. Local thermal equilibrium between solid matrix, gas and liquid phases is assumed.

In the partially saturated zones liquid water is separated from the gas phase by a meniscus. Due to the curvature of this meniscus the equilibrium equation gives the relationship $p^c = p^g - p^w$ between the capillary pressure $p^c(\mathbf{x},t)$, the gas pressure $p^g(\mathbf{x},t)$ and the water pressure $p^w(\mathbf{x},t)$. The state of the medium is assumed to be described by capillary pressure, gas pressure, absolute temperature $T(\mathbf{x},t)$ and displacements of the solid matrix $\mathbf{u}(\mathbf{x},t)$. For a detailed discussion about the chosen primary variables see Sanavia *et al.*(2006). The motion of the solid is assumed as a reference, while that of the fluids is described with respect to the solid.

The macroscopic balance equations of the model are now developed in the geometrically linear framework by considering quasi-static deformation processes and including the dissolution of air in liquid water and air mass sources during its desorption at lower water pressure. This model is developed by extending the previous one neglecting the air dissolved in liquid water. Hence the final equations of the model are summarized below (the interested reader can refer to Lewis and Schrefler, 1999 and Schrefler, 2002 for the full development).

The linear momentum balance equation of the mixture in terms of modified effective Cauchy's stress $\boldsymbol{\sigma}'(\mathbf{x}, t)$ assumes the form, (Schrefler 1984; Schrefler and Gawin 1996; Lewis and Schrefler 1998)

$$\text{div}\left(\boldsymbol{\sigma}' - [p^g - S_w p^c] \mathbf{1}\right) + \rho \mathbf{g} = \mathbf{0}, \quad (5)$$

where $\rho = [1 - n] \rho^s + n S_w \rho^w + n S_g \rho^g$ is the density of the mixture, $n(\mathbf{x},t)$ the porosity, $S_w(\mathbf{x},t)$ and $S_g(\mathbf{x},t)$ the water and gas degree of saturation, respectively, \mathbf{g} is the gravity acceleration vector and $\mathbf{1}$ the second order identity tensor.

The mass conservation equation for liquid water and water vapour is (Gawin and Schrefler 1996; Lewis and Schrefler 1998),

$$\begin{aligned}
& n[\rho^w + \rho^{gw}] \frac{\partial S_w}{\partial t} + [\rho^w S_w + \rho^{gw} S_g] \operatorname{div} \mathbf{v}^s + n S_g \frac{\partial \rho^{gw}}{\partial t} \\
& - \operatorname{div} \left(\rho^g \frac{M_a M_w}{M_g^2} \mathbf{D}_g^{gw} \operatorname{grad} \left(\frac{p^{gw}}{p^g} \right) \right) - \operatorname{div} \left(\rho^w \frac{\mathbf{k}k^{rw}}{\mu^w} [\operatorname{grad}(p^g) - \operatorname{grad}(p^c) - \rho^w \mathbf{g}] \right) \\
& - \operatorname{div} \left(\rho^{gw} \frac{\mathbf{k}k^{rg}}{\mu^g} [\operatorname{grad}(p^g) - \rho^g \mathbf{g}] \right) - \beta_{swg} \frac{\partial T}{\partial t} = 0,
\end{aligned} \tag{6}$$

where $\mathbf{k}(\mathbf{x}, t)$ is the intrinsic permeability tensor [m^2], $k^{rw}(\mathbf{x}, t)$ the water relative permeability parameter and $\mu^w(\mathbf{x}, t)$ the dynamic viscosity of water. Similarly, $k^{rg}(\mathbf{x}, t)$ is the gas relative permeability parameter and $\mu^g(\mathbf{x}, t)$ the dynamic viscosity of gas. $\beta_{swg}(\mathbf{x}, t)$ combines the solid and liquid cubic thermal expansion coefficients ($\beta_{swg} = [1-n]\beta_s[S_g \rho^{gw} + \rho^w S_w]$). \mathbf{D}_g^{gw} is the effective diffusivity tensor of water vapour in dry air, and M_a , M_w and $M_g(\mathbf{x}, t)$ the molar mass of dry air, liquid water and gas mixture, respectively. In equation (6) Fick's law has been used to describe the non-advective flow, while advective flows are modelled with Darcy's law.

The mass balance equation for dry air is:

$$\begin{aligned}
& -n \rho^{ga} \frac{\partial S_w}{\partial t} + \rho^{ga} S_g \operatorname{div} \mathbf{v}^s + n S_g \frac{\partial \rho^{ga}}{\partial t} - \operatorname{div} \left(\rho^g \frac{M_a M_w}{M_g^2} \mathbf{D}_g^{ga} \operatorname{grad} \left(\frac{p^{ga}}{p^g} \right) \right) + \\
& - \operatorname{div} \left(\rho^{ga} \frac{\mathbf{k}k^{rg}}{\mu^g} [\operatorname{grad}(p^g) - \rho^g \mathbf{g}] \right) - \beta_s \rho^{ga} (1-n) S_g \frac{\partial T}{\partial t} = \dot{m}_{ga}.
\end{aligned} \tag{7}$$

where \mathbf{D}_g^{ga} is the effective diffusivity tensor of dry air in water vapour, $\beta_s(\mathbf{x}, t)$ the solid cubic thermal expansion coefficient and \dot{m}_{ga} is a source term representing the rate of mass released in the gas phase by desorption of dissolved air at lower water pressure. This source term is zero when neglecting the air dissolved in liquid water. When considered it is given by the mass balance of dissolved air:

$$\begin{aligned}
& n \rho^w c_{wa} \frac{\partial S_w}{\partial t} + \rho^w c_{wa} S_w \operatorname{div} \mathbf{v}^s - \operatorname{div} \left(\rho^w \mathbf{D}_w^{ga} \operatorname{grad}(c_{wa}) \right) + n \rho^w S_w \frac{\partial c_{wa}}{\partial t} \\
& - \operatorname{div} \left(c_{wa} \rho^w \frac{\mathbf{k}k^{rw}}{\mu^w} [\operatorname{grad}(p^g) - \operatorname{grad}(p^c) - \rho^w \mathbf{g}] \right) - c_{wa} \beta_{swg} \frac{\partial T}{\partial t} = -\dot{m}_{ga},
\end{aligned} \tag{8}$$

where $c_{wa}(\mathbf{x}, t)$ is the concentration of air dissolved in water and \mathbf{D}_w^{ga} the effective diffusivity tensor of dissolved air in liquid water.

The last balance equation of the model is the energy balance equation of the mixture, here written as (Gawin and Schrefler 1996; Lewis and Schrefler 1998):

$$\left(\rho C_p\right)_{eff} \frac{\partial T}{\partial t} + \left(\rho_w C_p^w \mathbf{v}^w + \rho_g C_p^g \mathbf{v}^g\right) \cdot \mathbf{grad} T - \operatorname{div}\left(\chi_{eff} \mathbf{grad} T\right) = -\dot{m} \Delta H_{vap}, \quad (9)$$

where $\left(\rho C_p\right)_{eff}$ is the effective thermal capacity of porous medium, C_p^w and C_p^g the specific heat of water and gas mixture, respectively, χ_{eff} the effective thermal conductivity of the porous medium and the right hand term considers the contribution of the evaporation and condensation. This balance equation takes into account the heat transfer through conduction and convection as well as latent heat transfer (see Gawin and Schrefler 1996; Lewis and Schrefler 1998) and neglects the terms related to the mechanical work induced by density variations due to temperature changes of the phases and induced by volume fraction changes. A more general balance equation can be found in the work of Khalili and Loret (2001).

The model developed so far is composed by five balance equations, for which five state variables are needed. This model can be simplified when water flow in a fully saturated porous material is analyzed. In such a case, all the terms in equation (6) related to water vapour are equal to zero and can be omitted. Similar situation occurs also in a material where the saturation degree is very close to one (e.g. during initial stages of water outflow from fully saturated porous media) and the mass transport related to water vapour is very small in comparison to the liquid water flow and can be omitted. Multiplying the ‘reduced’ equation (6) (i.e. without the vapour-related terms) by the dissolved air concentration, c_{wa} , and then subtracting it from equation (8) one obtains,

$$\begin{aligned} & -\operatorname{div}\left[\rho^w \mathbf{D}_w^{ga} \mathbf{grad}\left(c_{wa}\right)\right] + n \rho^w S_w \frac{\partial c_{wa}}{\partial t} \\ & -\mathbf{grad}\left(c_{wa}\right) \cdot \left(\rho^w \frac{\mathbf{k} \mathbf{k}^{rw}}{\mu^w} \left[\mathbf{grad}\left(p^g\right) - \mathbf{grad}\left(p^c\right) - \rho^w \mathbf{g}\right]\right) = -\dot{m}_{ga}. \end{aligned} \quad (10)$$

The latter equation, with the assumption that the gradient of dissolved air concentration is small enough to neglect effects of both the diffusive and advective flows of dissolved air, i.e. $\mathbf{grad}\left(c_{wa}\right) \cong 0$, reduces to,

$$\dot{m}_{ga} = -n \rho^w S_w \frac{\partial c_{wa}}{\partial t}. \quad (11)$$

This assumption is reasonable when analyzing transient flows in porous materials, with the characteristic times smaller than those for diffusion or advection processes of the air dissolved in water.

Considering the Henry law for water within porous materials in fully saturated state, in its simplified form (3), one obtains

$$\dot{m}_{ga} = -\frac{n\rho^w S_w}{K_{wa}} \frac{\partial p^w}{\partial t}. \quad (12)$$

This defines the source term of the RHS of the mass balance equation (7). The latter equation makes any physical sense only when air occupies a part of the pores' volume, i.e. $S_w < 1$. The latter condition is however not fulfilled for a fully saturated material. For this reason, to analyse release of the air dissolved in pore water within fully saturated materials, where water pressure is higher than or equal to atmospheric pressure, $p^w \geq p_{atm}$, it is necessary to introduce some 'residual' gas saturation degree, $S_g^{res} > 0$. Such a technique is sometimes used during modelling of 'full - partial saturation' transition, and it was shown to give results in a good agreement with the experimental data of Liakopoulos (1965), (Gawin and Schrefler 1996; Gawin *et al.* 1997). This method will be also used in Section 5 to analyse numerically the effects of dissolved air on the hygral performance of water saturated dense sands during water pressure decrease within dilatant shear bands.

4.1. Constitutive equations

To close the previous model a sufficient number of suitable constitutive relationships have to be introduced. For the gas phase, the ideal gas law is used because the moist air is assumed to be a perfect mixture of two ideal gases. The equation of state of perfect gas (Clapeyron's equation) and Dalton's law are applied to dry air (ga), water vapour (gw) and moist air (g). In the partially saturated zones, the equilibrium water vapour pressure $p^{sw}(\mathbf{x}, t)$ can be obtained from the Kelvin-Laplace equation, where the water vapour saturation pressure, depending only upon the temperature, can be calculated from the Clausius-Clapeyron equation or from an empirical correlation.

The saturation degree $S_\pi(\mathbf{x}, t)$ and the relative permeability $k^{\pi}(\mathbf{x}, t)$ are experimentally determined functions of the capillary pressure and the temperature ($\pi = w, g$).

The solid skeleton is assumed elasto-plastic, homogeneous and isotropic; its mechanical behaviour is described within the classical rate-independent elasto-plasticity theory for geometrically linear problems. The yield function restricting the effective stress state $\boldsymbol{\sigma}'(\mathbf{x}, t)$ is developed in the form of temperature independent Drucker-Prager for simplicity, with linear

isotropic softening and non-associated plastic flow to take into account the post-peak and dilatant behaviour of dense sands, respectively. The return mapping and the consistent tangent operator is developed in the work of Sanavia *et al.* (2006), solving the singular behaviour of the Drucker-Prager yield surface in the zone of the apex using the concept of multi-surface plasticity following the formulation developed by Sanavia *et al.* (2002) for isotropic linear hardening/softening and volumetric-deviatoric non-associative plasticity in case of large strain elasto-plasticity.

In this paper, the effect of the capillary pressure and temperature on the evolution of the yield surface is not taken into account. The interested reader can refer, for example, to Alonso *et al.* (1990), Bolzon *et al.* (1996), Borja (2004) and François and Laloui (2008) for capillary dependent constitutive relationships in isothermal or non isothermal conditions and to Zhang *et al.* (2001) for the numerical implementation of constitutive law proposed by Bolzon *et al.* (1996) and its application to strain localization analysis.

4.2. Initial and boundary conditions

The initial conditions specify the full fields of primary state variables at the reference time $t=t_0$, in the whole domain and on its boundary as: $p^g = p_0^g$, $p_c = p_0^c$, $T = T_0$, $\mathbf{u} = \mathbf{u}_0$ on $B \cup \partial B$.

The boundary conditions (BCs) can be of Dirichlet's type on ∂B_π for $t \geq t_0$:

$$p^g = \hat{p}^g \text{ on } \partial B_g, \quad p^c = \hat{p}^c \text{ on } \partial B_c, \quad T = \hat{T} \text{ on } \partial B_T, \quad \mathbf{u} = \hat{\mathbf{u}} \text{ on } \partial B_u \quad (13)$$

or of Neumann' BCs type on ∂B_π^q for $t \geq t_0$:

$$\begin{aligned} (\rho^{ga} \mathbf{v}^g - \rho^g \mathbf{v}^{gw}) \cdot \mathbf{n} &= q^{ga} \quad \text{on } \partial B_g^q, \\ (\rho^{gw} \mathbf{v}^g + \rho^w \mathbf{v}^w + \rho^g \mathbf{v}^{gw}) \cdot \mathbf{n} &= \beta_c (\rho^{gw} - \rho_\infty^{gw}) + q^{gw} + q^w \quad \text{on } \partial B_c^q, \\ -(\rho^w \mathbf{v}^w \Delta h_{vap} - \lambda_{eff} \nabla T) \cdot \mathbf{n} &= \alpha_c (T - T_\infty) + q^T \quad \text{on } \partial B_T^q, \\ \boldsymbol{\sigma} \cdot \mathbf{n} &= \mathbf{t} \quad \text{on } \partial B_u^q, \end{aligned} \quad (14)$$

where $\mathbf{n}(\mathbf{x}, t)$ is the unit normal vector, pointing toward the surrounding gas, $q^{ga}(\mathbf{x}, t)$, $q^{gw}(\mathbf{x}, t)$, $q^w(\mathbf{x}, t)$ and $q^T(\mathbf{x}, t)$ are the imposed fluxes of dry air, vapour, liquid water and the imposed heat flux, respectively, and $\mathbf{t}(\mathbf{x}, t)$ is the imposed traction vector related to the total Cauchy stress tensor $\boldsymbol{\sigma}(\mathbf{x}, t)$; $\rho_\infty^{gw}(\mathbf{x}, t)$ and $T_\infty(\mathbf{x}, t)$ are the mass concentration of water vapour and the temperature in the far field of undisturbed gas phase, while $\alpha_c(\mathbf{x}, t)$ and $\beta_c(\mathbf{x}, t)$ are convective heat and mass exchange coefficients.

The boundary conditions for the dissolved air are not needed because we use the mass balance equation (7) with the RHS term in its simplified form, i.e. equation (12).

5 Numerical solution

The finite element model is derived by applying the Galerkin procedure for spatial integration and the Generalised Trapezoidal Method for time integration of the weak form of the balance equations of Section 4. A non-symmetric, non-linear and coupled system of equation is obtained (implicit one-step time integration has been used). Owing to the strong coupling between the mechanical and the pore fluids fields, a monolithic solution of the discretized equations system is preferred using a Newton-Rapson scheme (e.g. Bianco *et al.* 2003). Details concerning the matrices and the residuum vector of the linearized equations system of the finite element model without considering dissolved air (i.e. the source RHS term of equation (7)) can be found in the work of Sanavia *et al.* (2006).

In the following, an example of rapid desaturation of initially water saturated porous media is analysed with the appropriately modified computer code Comes-Geo (Gawin and Schrefler, 1996; Sanavia *et al.*, 2006) where the model developed in the previous sections has been implemented.

The example was previously solved by Sanavia *et al.* (2006) without considering the effects of air dissolved in pore water. It is inspired by the undrained plane strain biaxial compression test on dense sands, (Mokni and Desrues, 1998), where strain localization and cavitation of the pore water were experimentally observed.

Here the example is simulated with the numerical model considering the effects of air dissolved in liquid water (case 2) and neglecting them (case 1).

The rectangular sample of homogeneous soil of 34 cm height and 10 cm width has been discretized using a regular mesh of 340 eight-node elements, Figure 5. The material was initially fully saturated with water and the boundaries of the sample were impervious and adiabatic. Imposed vertical displacements were applied on the top surface with the constant rate of 1.2 mm/s. Vertical and horizontal displacements were constrained at the bottom surface. Plane strains and quasi-static loading conditions were assumed.

The initial temperature in the sample was constant and fixed at the ambient value (i.e. 20°C). Gravity forces were taken into account. The mechanical behaviour of the solid skeleton was simulated using the elasto-plastic Drucker-Prager constitutive model, with isotropic linear softening behaviour as phenomenological description of damage effects and

non-associated plastic flow. The material parameters used in the computation are listed in Table 1.

The constitutive relationships for the water degree of saturation $S_w(p^c)$ and water relative permeability $k^{rw}(S_w)$ were those of Safai and Pinder (1979) in isothermal conditions. For the gas relative permeability $k^{rg}(S_w)$, the relationship of Brooks and Corey (1966) in isothermal conditions has been assumed. These relationships have been used for sake of simplicity because of the lack of experimental data.

Figure 5 and Table 1

In the finite element analysis, the dilatant behaviour of dense sands is simulated selecting a positive value of the angle of dilatancy (20°). For this material in samples with impervious boundary, the increment of void ratio due to the dilatant behaviour of dense sand is modelled through volumetric plastic deformations and causes a drop of water pressure. As a result, cavitation may develop when water pressure equal to the saturation vapour pressure at the temperature of the sample is reached (i.e. $p_{vsat} = 2338$ Pa at $T=20^\circ\text{C}$).

The results of simulations for the two considered cases are presented below as the contours in the entire domain at the end of the simulations and the time histories in two nodal points, inside and outside the shear bands (the position of these points is indicated in Figure 6). For both analysed cases, the numerical results indicate the pronounced accumulation of inelastic strains in narrow zones, as it can be observed in Figure 6, where the equivalent plastic strain contours at the end of the numerical simulation are depicted.

For both considered cases, the volumetric strain (Figure 7a) emphasizes the dilatant behaviour of the shear bands because positive values develop only inside the plastic zones, while the negative values are observed in the elastic domain (Figure 7b). As a consequence, water pressure decreases inside the plastic zones up to the development of negative water pressures, i.e. capillary pressures higher than zero exist, as depicted in Figure 8a. At these conditions a vapour phase appears (i.e. water cavitation starts) because the water pressure decreases below the saturation vapour pressure at ambient temperature of 2338.8 Pa (see Figures 9 and 10) and a gradual water desaturation in the strain localization bands initiates (Figure 8b). Cavitation of water is hence described directly by the model, as shown in Figures 9 and 10, where it can be observed that the vapour phase appears only inside the dilatant plastic zones (in the model, vapour pressure equal to the saturation values, $p^v = p^{vs}$, means relative humidity equal to

100%RH and full saturation with water, while $p^v < p^{vs}$ means partial saturation). At the same time, the shear bands become partially saturated, as it can be seen in Figures 8b and 11.

When the dissolved air is considered in the mathematical model (case 2), a decrease of water pressure inside the plastic zones causes release of the dissolved air there, see Figure 12, which visibly accelerates, as compared to case 1, the increase of capillary pressure and the initiation of cavitation and desaturation processes, about 12 s for the considered example, (Figures 8a, 9 and 8b). One should underline that this happens at much lower values of the volumetric strain, despite of its' very similar evolution for the both considered cases, Figure 7a. The shear bands start at the same time, but, when cavitation develops, they have different time evolutions (Figure 7b) due to the change of effective stresses (equation 5). Hence, by using the developed model, one may conclude that considering the air dissolved in pore water is of importance when water cavitation in saturated porous media is analyzed.

Figures 6 – 12

For the aspects of the regularization properties of the multiphase models at strain localization, due to the pore fluids viscosity, the interested reader can see, e.g., Schrefler *et al.* (1996), Ehlers and Volk, (1999), Zhang *et al.* (1999), Schrefler *et al.* (1999), Benallal and Comi, (2004), Schrefler *et al.* (2006), and Zhang *et al.* (2007). Here the main emphasis is given on the analysis of the effect of the dissolved air released during desaturation due to cavitation. In the numerical example solved in this work, the shear band width is fixed by the element size, which was selected close to the experimental band width.

Conclusions

A coupled mathematical model for the hydro-thermo-mechanical behaviour of saturated and partially saturated porous media was extended to consider in a simplified way the effects of air dissolved in water. Physics of air dissolution and water cavitation in porous media were briefly discussed. Numerical solution of the model equations is used to analyze an undrained plane strain biaxial test where cavitation took place. It was shown that considering the dissolved air is of importance during simulation of cavitation in water saturated dense sands.

Acknowledgements

The authors would like to thank the University of Padua, Italy, (research grants: *UNIPD 60A09-5407/06* and *CPDA 048959/2004*) for the financial support.

References

- Alonso, E.E., Gens, A., Josa, A.: A constitutive model for partially saturated soils. *Géotechnique*. 40, 403-430 (1990)
- Atkins, P., de Paula, J.: *Atkins' Physical Chemistry*. Seventh Edition, Oxford University Press, New York (2002)
- Baur, T., Köngeter, J., Leucker, R.: Effects of dissolved gas on cavitation inception in free surface flows. In: J.M. Michel et al. (ed.) *Proceedings of the Third International Symposium on Cavitation: Cavitation 98*. Grenoble, France. Vol. 1, pp. 155-159, April 7-10, 1998
- Benallal, A., Comi, C.: On numerical analysis in the presence of unstable saturated porous materials. *International Journal for Numerical Methods in Engineering*. 56, 883-910 (2003)
- Bianco, M., Bilardi, G., Pesavento, F., Pucci, G., Schrefler, B.A.: A frontal solver tuned for fully coupled non-linear hygro-thermo-mechanical problems. *Int. J. Numer. Meth. Engng*. 57, 1801-1818 (2003)
- Bolzon, G., Schrefler, B.A., Zienkiewicz, O.C.: Elastoplastic soil constitutive laws generalized to partially saturated states. *Géotechnique*. 46, 279-289 (1996)
- Borja, R. I.: Cam-Clay plasticity. Part V: A mathematical framework for three-phase deformation and strain localization analyses of partially saturated porous media. *Computer Methods in Applied Mechanics and Engineering*. 193, 5301-5338 (2004)
- Brooks, R.N., Corey, A.T.: Properties of porous media affecting fluid flow. *Journal of Irrigation Drain. Division of the American Society of Civil Engineering*. 92(IR2), 61-68 (1966)
- Chambon, R., Desrues, J., Charlier, R., Hammad W.: CLoE, a new rate type constitutive model for geomaterials: theoretical basis and implementation. *Int. J. for Numerical and Analytical Methods in Geomechanics*. 18(4), 253-278 (1994)
- Ehlers, W., Volk, W.: Localization Phenomena in Liquid-Saturated and Empty Porous Solids. *Transport in Porous Media*. 34, 159-177 (1999)
- Ehlers, W., Graf, T., Ammann, M.: Deformation and localization analysis of partially saturated soil. *Computer Methods in Applied Mechanics and Engineering*. 193, 2885-2910 (2004)
- Gawin, D., Schrefler, B.A.: Thermo- hydro- mechanical analysis of partially saturated porous materials. *Engineering Computations*. 13(7), 113-143 (1996)
- Gawin, D., Simoni, L., Schrefler, B.A.: Numerical model for hydro-mechanical behaviour in deformable porous media: a benchmark problem. In: Jian-Xin Yuan (eds) *Computer methods and advances in Geomechanics*. Vol. 2, 1143-1148, Balkema, Rotterdam (1997)
- Gawin, D., Sanavia, L., Schrefler, B.A.: Cavitation modelling in saturated geomaterials with application to dynamic strain localisation. *Int. J. for Numerical Methods in Fluids*. 27, 109-125 (1998)

- Gens, A., Garcia-Molina, A.J., Olivella, S., Alonso, E.E., Huertas, F.: Analysis of a full scale in situ test simulating repository conditions. *Int. J. Numer. Anal. Meth. Geomech.* 22, 515-548 (1998).
- Habib, P: Production of gaseous pore pressure during rock slides. *Rock Mechanics.* 7, 193-197 (1975)
- Hassanizadeh, M., Gray, W.G.: General conservation equations for multi-phase system: 1. Averaging technique. *Advances in Water Resources.* 2, 131-144 (1979)
- Hendron, A.J. Patton, F.D.: The Vaiont slide, a geotechnical analysis based on new geologic observations of the failure surface, Technical Report GL-85-5. Washington DC, Department of the Army US Corps of Engineers vol. I (1985)
- Khalili, N., Loret, B.: An Elasto-Plastic Model for non-isothermal analysis of flow and deformation in unsaturated porous media: formulation. *Int. J. Solids and Structures.* 38: 8305-8330 (2001)
- Kwak, H.Y., Kim, Y.W.: Homogeneous nucleation and macroscopic growth of gas bubble in organic solutions. *Int. Heat Mass Transfer.* 41(4-5), 757-767 (1998)
- François, B., Laloui, L.: ACMEG-TS: a constitutive model for unsaturated soils under non-isothermal conditions. *Int. J. Numer. Anal. Meth. Geomech.* DOI: 10.1002/nag.712 (2008)
- LeBihan, J.P., Leroueil, S.: A model for gas and water flow through the core of earth dams. *Canadian Geotechnical Journal.* 39(1), 90-102 (2002)
- Lewis, R.W., Schrefler, B.A.: *The Finite Element Method in the Static and Dynamic Deformation and Consolidation of Porous Media.* J. Wiley, Chichester (1998)
- Liakopoulos, A.C.: *Transient flow through unsaturated porous media*, PhD thesis, University of California, Berkeley (CA), USA (1965)
- Maris, H., Balibar S.: Negative pressures and cavitation in liquid Helium. *Physics Today.* 53(2), 29-34 (2000)
- McManus, K.J., Davis, R.O.: Dilatation induced pore fluid cavitation in sands. *Géotechnique.* 47(1), 173-177 (1997)
- Mercury, L., Tardy, Y.: Negative pressure of stretched liquid water. *Geochemistry of soil capillaries. Geochimica et Cosmochimica Acta.* 65(20), 3391-3408 (2001)
- Mercury, L., Tardy, Y.: Response to the Comment by J. V. Walther on “Negative pressure of stretched liquid water. *Geochemistry of soil capillaries.*” (2001) *Geochim. Cosmochim. Acta* 65, 3391-3408; and “Thermodynamic properties of solutions in metastable systems under negative or positive pressures.” (2003) *Geochim. Cosmochim. Acta* 67, 1769-1785. *Geochimica et Cosmochimica Acta.* 68(12), 2775-2780 (2004)
- Mercury, L., Azaroual, M., Zeyen, H., Tardy, Y.: Thermodynamic properties of solutions in metastable systems under negative or positive pressures. *Geochimica et Cosmochimica Acta.* 67(10), 1769-1785 (2003)
- Mercury, L., Pinti, D.L., Zeyen, H.: The effect of negative pressure of capillary water on atmospheric noble gas solubility in ground water and palaeotemperature reconstruction. *Earth and Planetary Science Letters.* 223, 147-161 (2004)
- Mira, P., Pastor, M., Li, T., Liu, X.: Failure problems in soils: an enhanced strain coupled formulation with application to localization problems. *Revue française de génie civil.* 8, 735-759 (2004)

- Mokni, M., Desrues, J.: Strain localisation measurements in undrained plane-strain biaxial tests on Hostun RF sand. *Mechanics of Cohesive-Frictional Materials*. 4, 419-441 (1998)
- Olivella, S., Carrera, J., Gens A., Alonso, E.E.: Nonisothermal multiphase flow of brine and gas through saline media. *Transport in Porous Media*. 15, 271-293 (1994)
- Or, D., Tuller, M.: Cavitation during desaturation of porous media under tension. *Water Resources Research*. 38(5), 1061-1064 (2002)
- Rudnicki, J.W., Rice, J.R.: Conditions for the Localization of Deformation in Pressure-Sensitive Dilatant Materials. *Journal of the Mechanics and Physics of Solids*. 23, 371-394 (1975)
- Safai, N.M., Pinder, G.F.: Vertical and horizontal land deformation in a desaturating porous medium. *Advances in Water Resources*. 2, 19-25 (1979)
- Sanavia, L., Schrefler, B.A., Steinmann, P.: A formulation for an unsaturated porous medium undergoing large inelastic strains. *Computational Mechanics*. 28, 137-151 (2002)
- Sanavia, L., Pesavento, F., Schrefler, B.A.: Finite element analysis of non-isothermal multiphase geomaterials with application to strain localization simulation. *Computational Mechanics*. 37(4), 331-348 (2006)
- Schrefler, B.A.: *The Finite Element Method in Soil Consolidation (with applications to Surface Subsidence)*. PhD. Thesis, University College of Swansea, C/Ph/76/84, Swansea UK (1984)
- Schrefler, B.A.: *Mechanics and Thermodynamics of Saturated-Unsaturated Porous Materials and Quantitative Solutions*. *Applied Mechanics Review*. 55(4), 351-388 (2002)
- Schrefler, B.A., Gawin, D.: The effective stress principle: incremental or finite form? *Int. J. for Numerical and Analytical Methods in Geomechanics*. 20(11), 785-815 (1996)
- Schrefler, B.A., Majorana, C.E., Sanavia, L.: Shear band localisation in saturated porous media. *Archives of Mechanics*. 47, 577-599 (1995)
- Schrefler, B.A., Sanavia, L., Majorana, C.E.: A multiphase medium model for localisation and postlocalisation simulation in geomaterials. *Mechanics of Cohesive-Frictional Materials*. 1, 95-114 (1996)
- Schrefler, B.A., Zhang, H.W., Sanavia, L.: Fluid-structure interaction in the localisation of Saturated porous media. *ZAMM Zeitschrift für Angewandte Mathematik und Mechanik (Journal of Applied Mathematics and Mechanics)*. 79(7), 481-484 (1999)
- Schrefler, B.A., Zhang, H.W., Sanavia, L.: Interaction between different internal length scales in fully and partially saturated porous media - the 1-D case. *Int. J. for Numerical and Analytical Methods in Geomechanics*. 30, 45-70, (2006)
- Shuttle, D.A., Smith, I.M.: Localisation in the presence of excess pore-water pressure. *Computer and Geotechnics*. 9, 87-99 (1990)
- Tyree, M.T.: The Cohesion-Tension theory of sap ascent: current controversies. *Journal of Experimental Botany*. 48(315), 1753-1765 (1997)
- Vardoulakis, I.: Dynamic stability analysis of undrained simple shear on water-saturated granular soils. *Int. J. for Numerical and Analytical Methods in Geomechanics*. 10, 177-190 (1986)
- Vardoulakis, I., Sulem, J.: *Bifurcation Analysis in Geomechanics*. Blackie Academic & Professional (1995)

Zhang, H.W., Sanavia, L., Schrefler, B.A.: An internal length scale in dynamic strain localisation of multiphase porous media. *Mechanics of Cohesive-Frictional Materials*. 4, 443-460 (1999)

Zhang, H.W., Sanavia, L., Schrefler, B.A.: Numerical analysis of dynamic strain localisation in initially water saturated dense sand with a modified generalised plasticity model. *Computers and Structures*. 79, 441-459 (2001)

Zhang H.W., Qin J.M., Sanavia L., Schrefler B.A.: Some theoretical aspects of strain localization analysis of multiphase porous media with regularized constitutive models. *Mechanics of Advanced Materials and Structures*. 14(2), 107-130, (2007)

Zheng, Q., Durben, D.J., Wolf, G.H., Angell, C.A. Liquids at large negative pressures: Water at the homogeneous nucleation limit. *Science*. 254, 829–832 (1991)

Table 1. Material parameters assumed for dense sand in the example.

Material parameter	Value	Material parameter	Value
Porosity, [-]	0.2	Solid thermal conductivity, [W/(m·K)]	1.442
Intrinsic permeability, [m ²]	1.0 10 ⁻¹⁴	Solid specific heat, [J/(kg K)]	810.0
Solid skeleton density, [kg/m ³]	2000.0	Water viscosity, [Pa s]	1.0 10 ⁻³
Water density, [kg/m ³]	1000.0	Water heat conductivity, [W/(m·K)]	0.6
Young's modulus, [MPa]	30.0	Water vapour heat capacity, [J/(kg·K)]	1805
Poisson's ratio, [-]	0.4	Water vapour heat conductivity, [W/(m·K)]	0.0186
Apparent cohesion, [MPa]	0.5	Gravity acceleration, [m/s ²]	9.80665
Plastic modulus, [MPa]	-1.0	Irreducible saturation point, [-]	0.21
Internal friction angle, [deg]	30°	Critical saturation point, [-]	0.909
Dilatancy angle, [deg]	20°	Cubic thermal expansion coefficient, [K ⁻¹]	0.9 10 ⁻⁴
Solid matrix heat conductivity, [W/(m K)]	2.5		

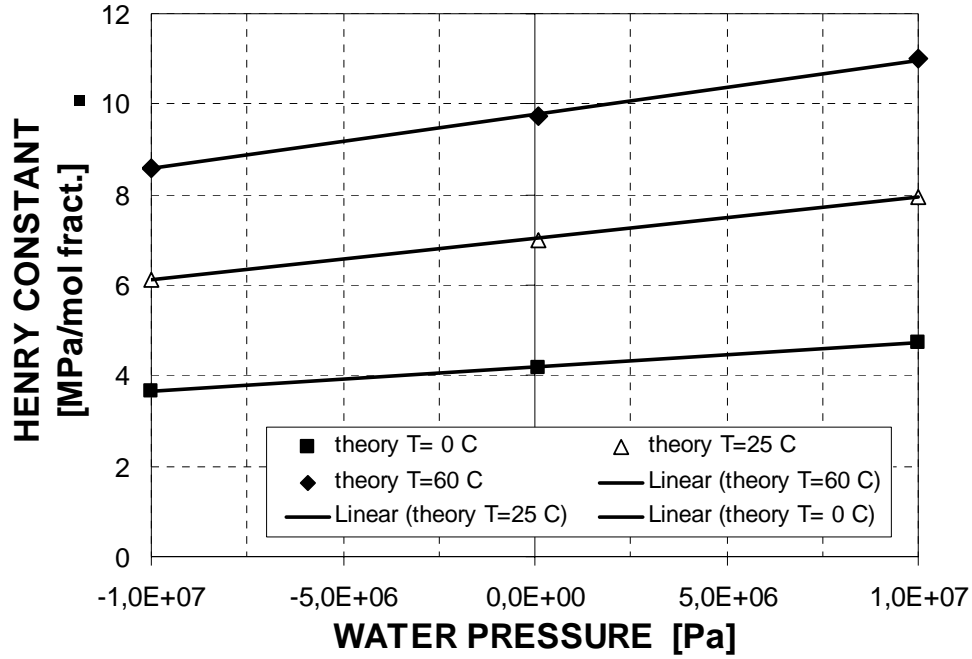


Figure 1. Theoretical values of Henry's law constants (Mercury *et al.*, 2003) for dry air at different temperatures and pressures of water, and their linear approximations.

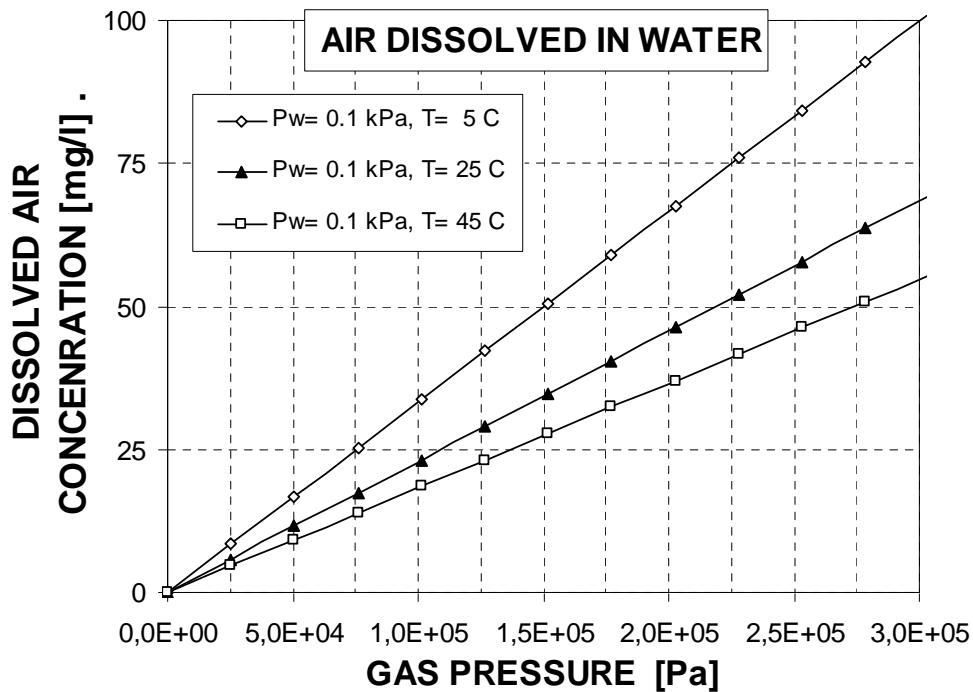


Figure 2. Dependence of the concentration of air dissolved in liquid water upon air pressure, for different values of pressure and temperature of water.

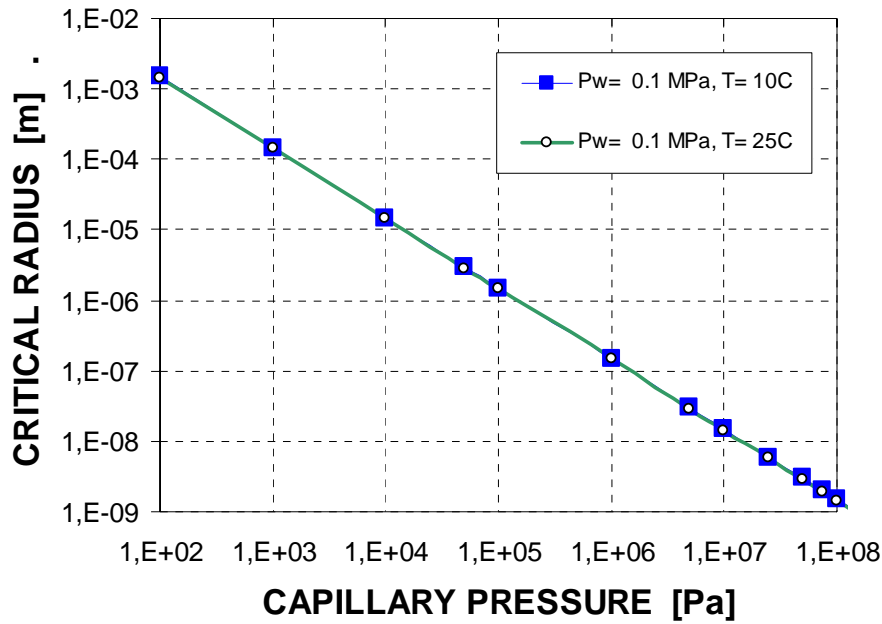


Figure 3. The critical radius of an air bubble in water at two temperatures, $T=10^{\circ}\text{C}$ (thin line) and $T=25^{\circ}\text{C}$ (solid line), and two values of water pressure, ($p^w=0.1\text{ MPa}$), as a function of the capillary pressure.

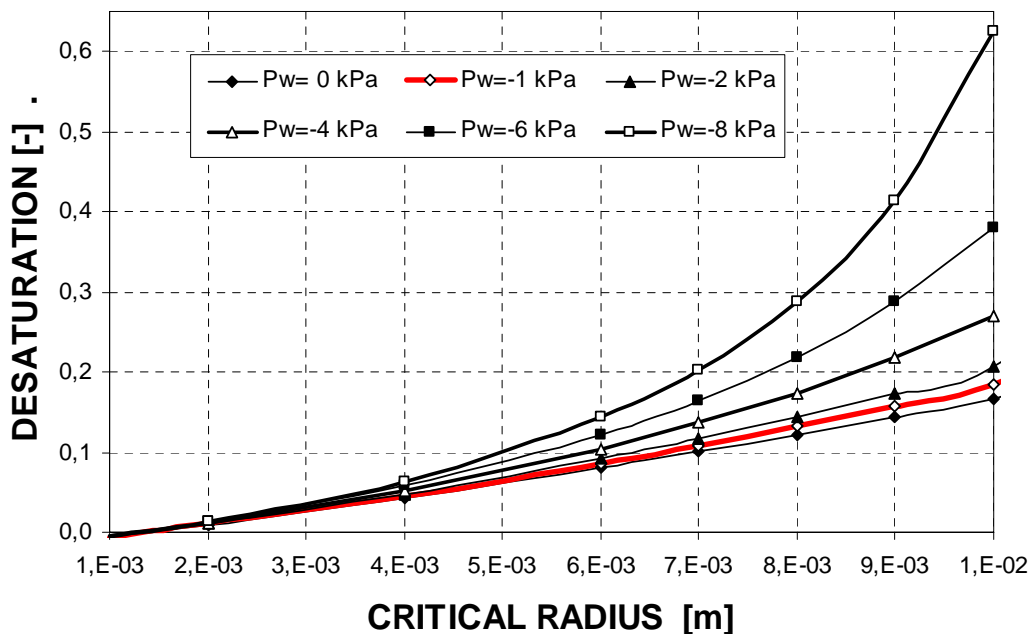


Figure 4. Additional pores desaturation caused by the dissolved air desorption into bubbles of different sizes from stretched water at temperature of 298.15 K (25°C) and different water pressures, from -8 kPa to 0 kPa .

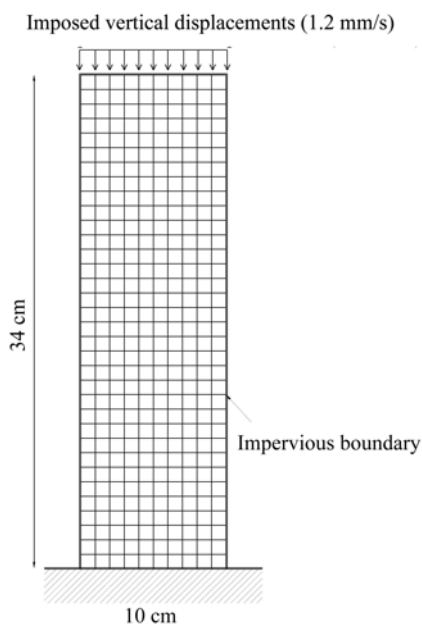


Figure 5. Geometry and boundary conditions for the numerical example.

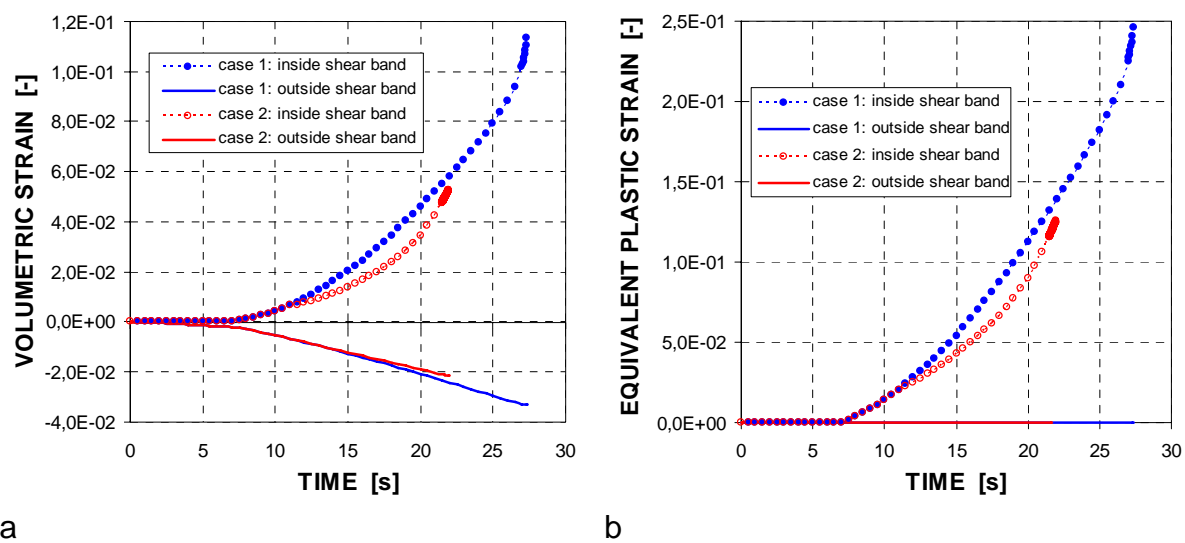
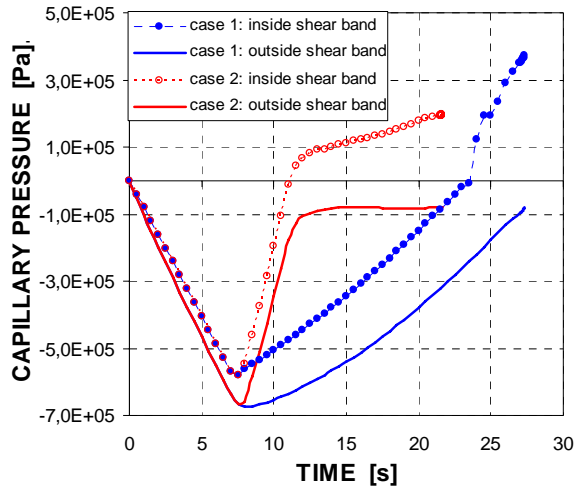
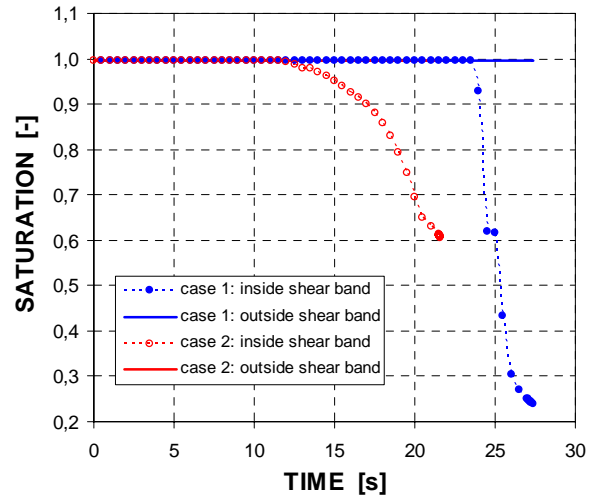


Figure 7. Comparison of the numerical simulation results in the points inside and outside the strain localisation band, obtained with the model neglecting (case 1) and considering the effects of the air dissolved in water (case 2):

a) Volumetric strain vs. time, b) Equivalent plastic strain vs. time.



a



b

Figure 8. Comparison of the numerical simulation results in the points inside and outside the strain localisation band, obtained with the model neglecting (case 1) and considering the effects of the air dissolved in water (case 2):

a) Capillary pressure vs. time, b) Saturation degree vs. time.

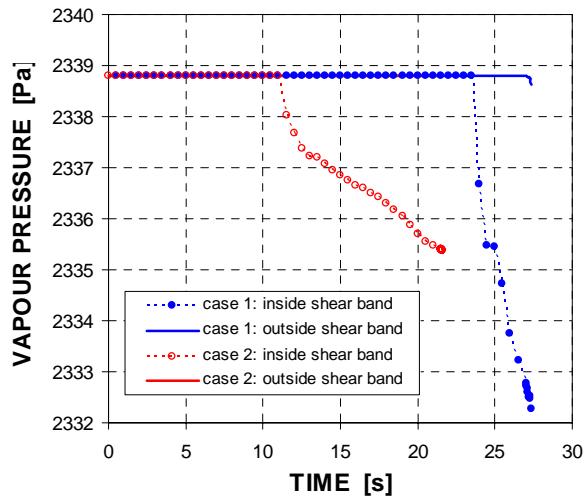


Figure 9. Comparison of vapour pressure vs. time in the points inside and outside the strain localisation band, obtained with the model neglecting (case 1) and considering the effects of the air dissolved in water (case 2).

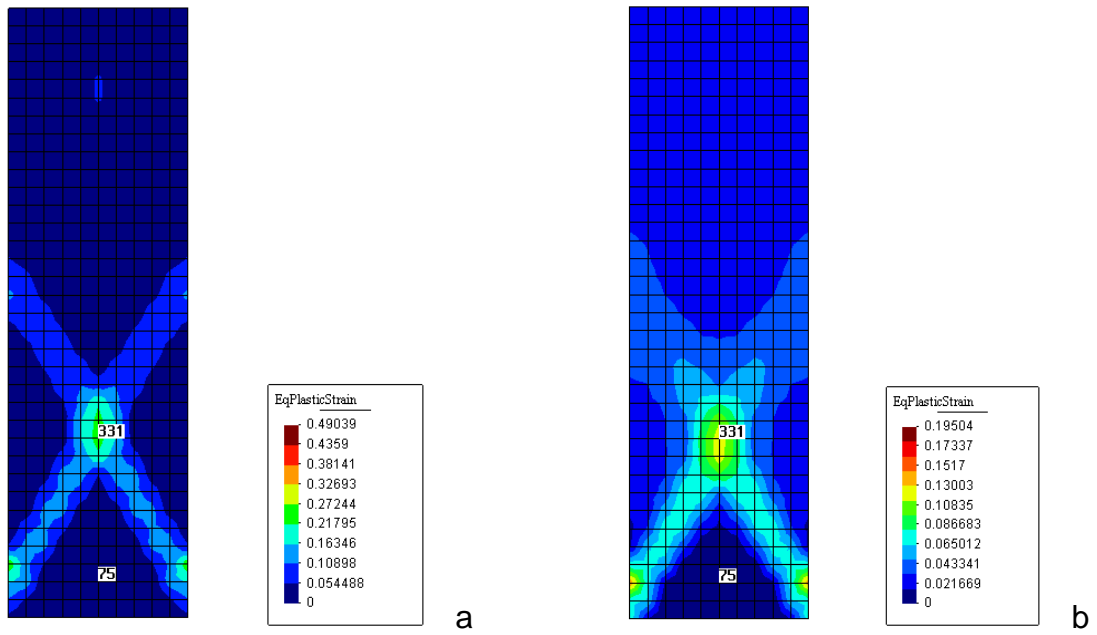


Figure 6. Equivalent plastic strain [-] contours obtained at the end of the numerical simulation with the model: a) neglecting the effects of the air dissolved in water (case 1) – $t=27.35$ s, b) considering these effects (case 2) – $t=22.0$ s, and position of the two nodal points of the Figures 9-11.

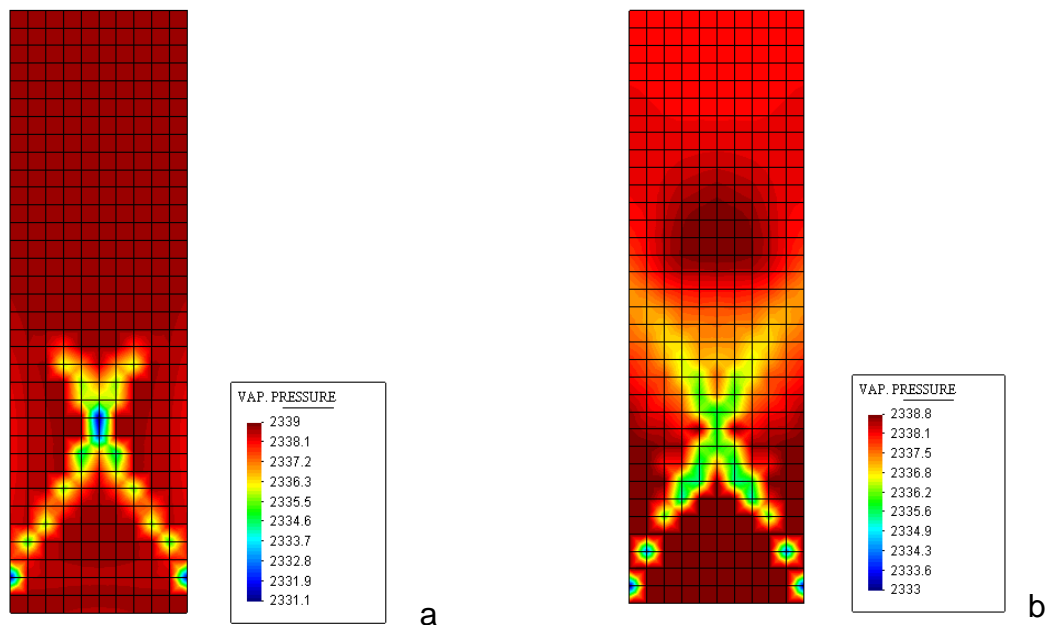


Figure 10. Vapour pressure [Pa] contours obtained at the end of the numerical simulation with the model: a) neglecting the effects of the air dissolved in water (case 1), b) considering these effects (case 2).

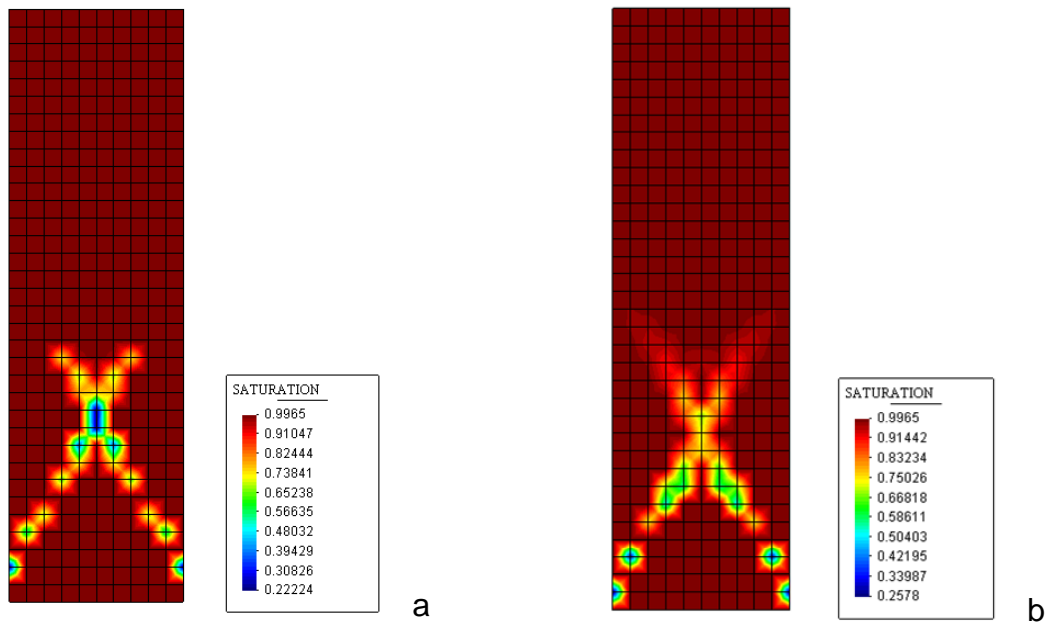


Fig. 11. Saturation degree [-] contours obtained at the end of the numerical simulation with the model: a) neglecting the effects of the air dissolved in water (case 1), b) considering these effects (case 2).

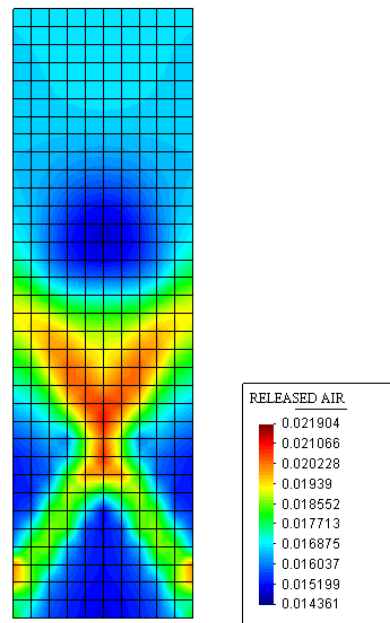


Figure 12. Contours of total amount of dissolved air released from the pore water [kg/m^3], obtained at the end of the numerical simulation ($t= 22.0$ s) with the model considering the effects of the air dissolved in water (case 2).